

**Supplementary Information For**  
**Distinctive Electronic Characteristics and Ultra-high**  
**Thermoelectric Power Factor in Be-Fe Intermetallics**

Qi D. Hao<sup>1,2</sup>, H. Wang<sup>2</sup>, Xiang R. Chen<sup>1\*</sup>, Hua Y. Geng<sup>2,3\*</sup>

<sup>1</sup> *College of Physics, Sichuan University, Chengdu 610065, P. R. China;*

<sup>2</sup> *National Key Laboratory of Shock Wave and Detonation Physics, Institute of Fluid Physics,  
China Academy of Engineering Physics, Mianyang, Sichuan 621900, P. R. China;*

<sup>3</sup> *HEDPS, Center for Applied Physics and Technology, and College of Engineering, Peking  
University, Beijing 100871, P. R. China;*

---

\* *Corresponding authors. E-mail: s102genghy@caep.cn; xrchen@scu.edu.cn*

## Supplementary Methods

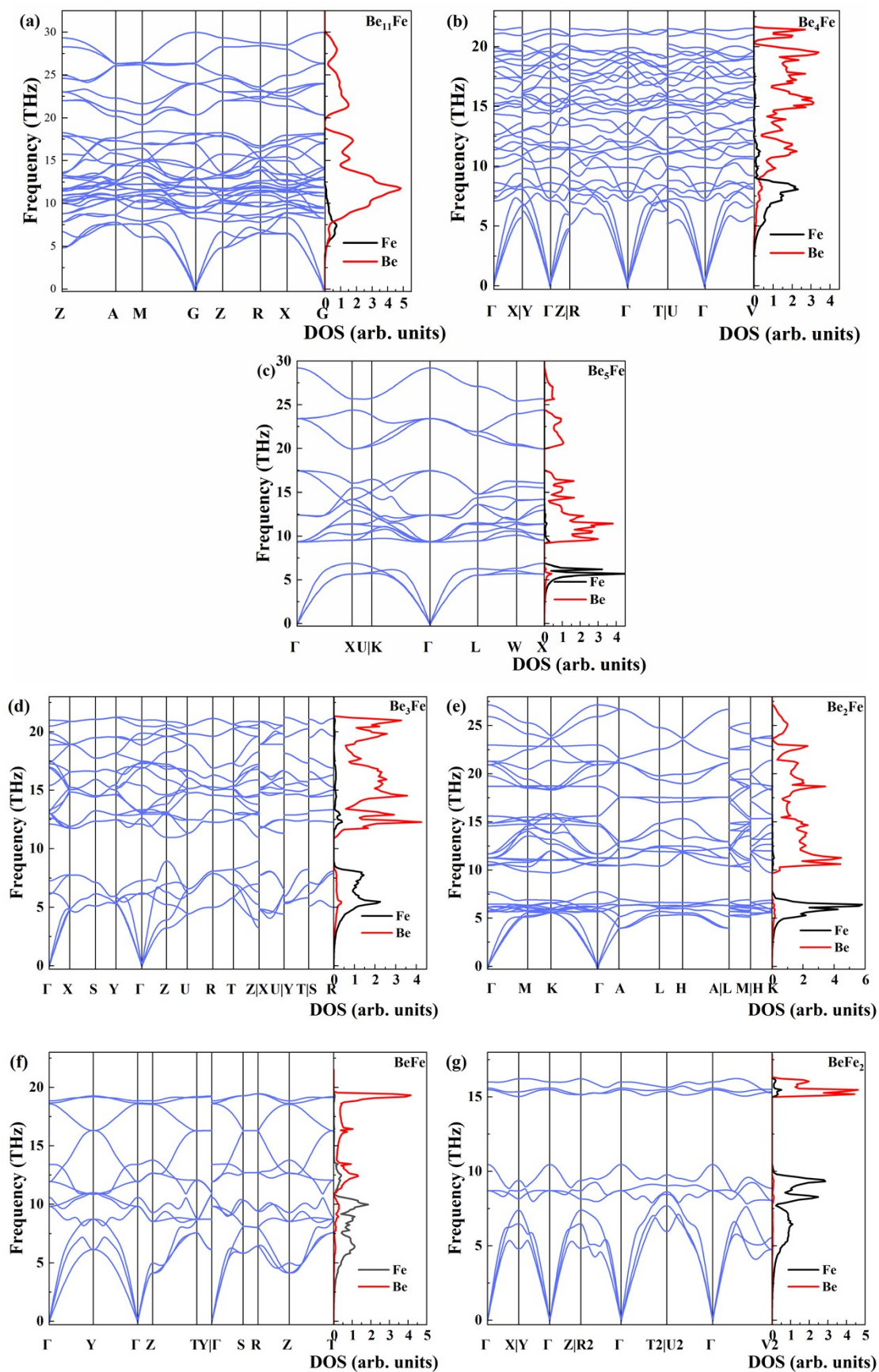
We performed two independent variable-composition structure searches using USPEX code[1] to find possible stable phases in Be-Fe system, covering a size of the system up to 28 atoms/cell. The maximal generation was set to 60. For each structure that might be stable, we performed higher precision calculations using VASP[2,3] again, where the employed structural relaxation criterion is that for the forces on each atom must be less than 0.001 eV/Å. The electronic SCF criterion was set to a tolerance of  $10^{-7}$  eV, the plane wave basis cut-off energy was set to 700 eV, and Monkhorst-Pack[4] k-meshes with a grid spacing of  $2\pi \times 0.016 \text{ \AA}^{-1}$  that including the  $\Gamma$  point were used. The formation enthalpy per atom of  $\text{Be}_x\text{Fe}_y$  was calculated by  $\Delta H(\text{Be}_x\text{Fe}_y)=[H(\text{Be}_x\text{Fe}_y)-xH(\text{Be})-yH(\text{Fe})]/(x+y)$ , where  $H$  is the total enthalpy. We also note that  $\text{Be}_{11}\text{Fe}$  has an enthalpy less than 4 meV/atom higher than the convex hull, which is too small to be distinguished with the accuracy of the available theoretical methods. We thus take it as a ground state in this work as well.

$G_0W_0$  calculations were performed on top of the PBE wavefunctions, where the energy cutoff for the response function was set to 350 eV. The plane wave cutoff energy (ENCUT) was set to 650 eV, and the maximum number of bands supported by this value was used for exact diagonalization of the Kohn-Sham Hamiltonian. For  $\text{Be}_{11}\text{Fe}$  and  $\text{Be}_4\text{Fe}$ , the Monkhorst-Pack k-meshes of  $9 \times 9 \times 7$  and  $8 \times 8 \times 6$  including the  $\Gamma$  point were used respectively. The Bader charge analysis data were calculated using a fine

Fast Fourier Transform grid of  $12 \times G_{cut}$  ( $G_{cut} = \frac{\sqrt{2m_e ENCUT}}{h}$ ), which is sufficient to

ensure the convergence of the Bader charge analysis for all phases. We calculated the lattice thermal conductivity using the ShengBTE code[5] by considering the influence of third-nearest neighbor atoms, where the required second- and third-order force constants were obtained using a  $2 \times 2 \times 2$  supercell. In DFPT calculations with QUANTUM ESPRESSO package[6], norm-conserving pseudopotentials were used, and as in VASP calculations,  $1s^2 2s^2$  of Be and  $3s^2 3p^6 4s^2 3d^6$  of Fe were treated as valence electrons. The kinetic energy cutoff for wavefunction expansion was set to 93 Ry, and q-points meshes of  $6 \times 6 \times 6$  and  $4 \times 4 \times 4$  were used for  $\text{Be}_{11}\text{Fe}$  and  $\text{Be}_4\text{Fe}$ , respectively. Although such accuracy is enough to obtain sufficiently accurate phonon frequencies, it is not fine enough for calculating the electron self-energy through the electron-phonon coupling theory. We thus further performed interpolation using EPW code[7] and finally executed the calculations on a  $30 \times 30 \times 30$  grid and obtained an imaginary part of the electron self-energy on a  $12 \times 12 \times 12$  k-points mesh. Then we performed a high-accuracy non-self-consistent calculation with VASP using a Monkhorst-Pack k-mesh with a grid spacing of  $2\pi \times 0.011 \text{ \AA}^{-1}$  to obtain the Kohn-Sham eigenvalues. Thanks to the Fourier interpolation module provided by the BoltzTraP2 program[8], We were able to conveniently interpolate the relaxation time and the Kohn-Sham eigenvalues together to a grid that has 45 times more k-points than the one used for calculating the Kohn-Sham eigenvalues, and the accurate electronic transport properties were then calculated.

## Supplementary Figures



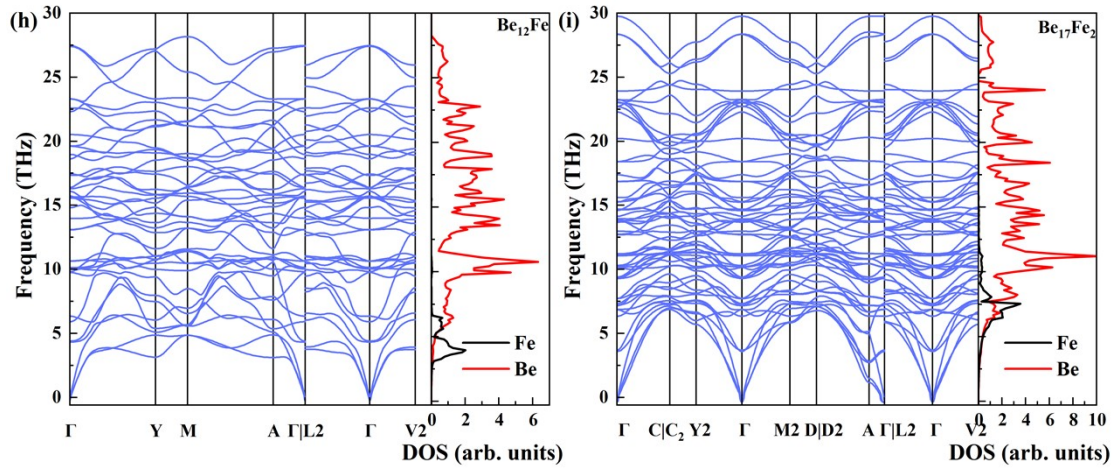


**Fig. S1.** (color online) Calculated phonon dispersion and projected phonon density of states of (a)  $\text{Be}_{11}\text{Fe}$ , (b)  $\text{Be}_4\text{Fe}$ , (c)  $\text{Be}_5\text{Fe}$ , (d)  $\text{Be}_3\text{Fe}$ , (e)  $\text{Be}_2\text{Fe}$ , (f)  $\text{BeFe}$ , (g)  $\text{BeFe}_2$ , (h)  $\text{Be}_{12}\text{Fe}$ , and (i)  $\text{Be}_{17}\text{Fe}_2$ , respectively.

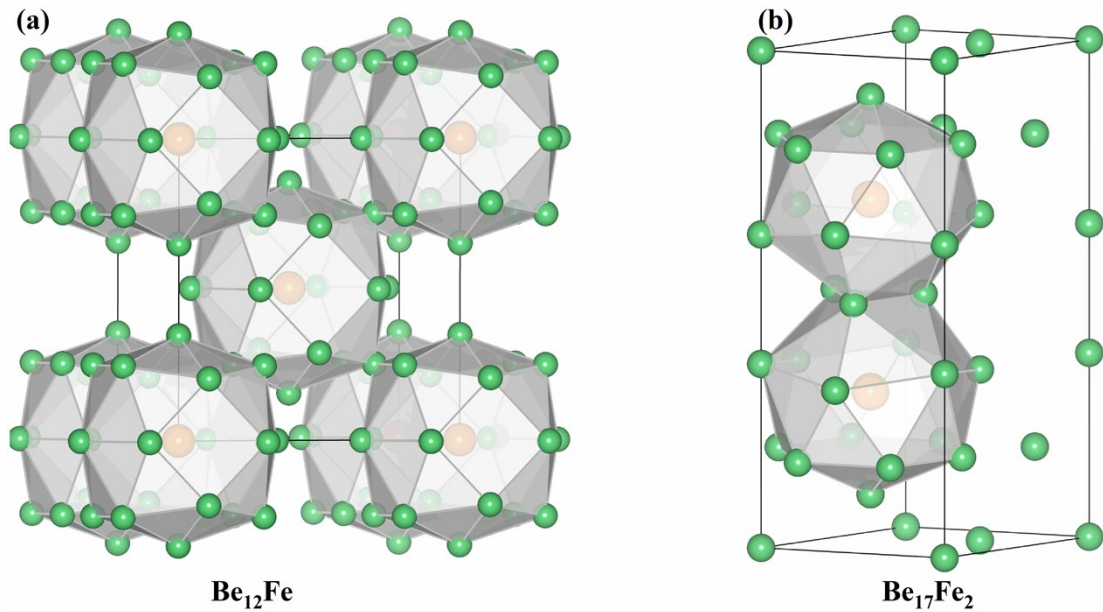


**Fig. S2.** (color online) The clathrate structures in  $\text{Be}_{12}\text{Fe}$  and  $\text{Be}_{17}\text{Fe}_2$ , where the Fe atoms in  $\text{Be}_{12}\text{Fe}$  are surrounded by 34-face cages formed by 20 Be atoms (a), and the Fe atoms in  $\text{Be}_{17}\text{Fe}_2$  are surrounded by 28-face cages formed by 16 Be atoms (b).

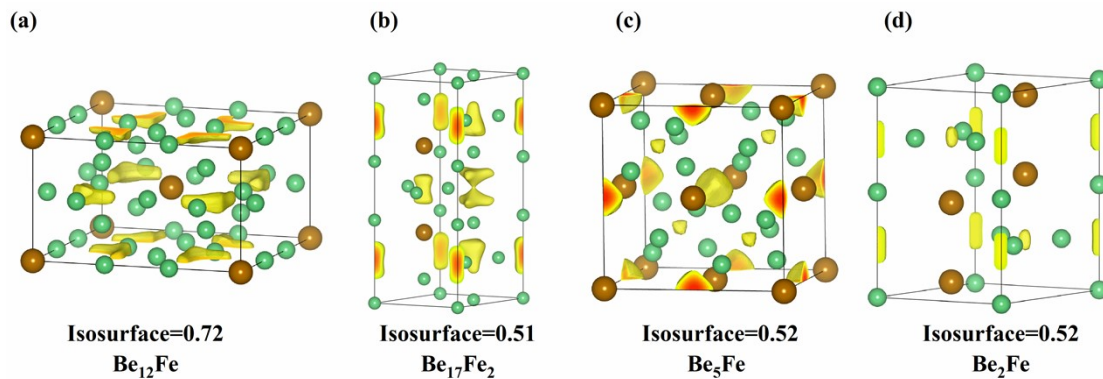


**Fig. S3.** (color online) The ELF of selected Be-Fe compounds: (a)  $\text{Be}_{12}\text{Fe}$ , (b)  $\text{Be}_{17}\text{Fe}_2$ , (c)  $\text{Be}_5\text{Fe}$ ,

and (d)  $\text{Be}_2\text{Fe}$ .

In Figs. S4 and S5, we show the characteristics of conventional ISQ and type-II ISQ using  $\text{Be}_{11}\text{Fe}$  and  $\text{Be}_2\text{Fe}$  as the example, respectively. The locations of ISQs in both  $\text{Be}_{11}\text{Fe}$  and  $\text{Be}_2\text{Fe}$  are the joint maxima of charge density and ELF in real space. Therefore they both are electricle according the “ELF+CHG” criterion. However, the difference is that the ELF value at the location of conventional ISQ is relatively high ( $> 0.6$ ), while the ELF of type-II ISQ is at a level of  $\sim 0.5$  and does not exceed 0.6. The low ELF of type-II ISQ indicates the electrons accumulated in these interstitial regions will flow in and out continually.

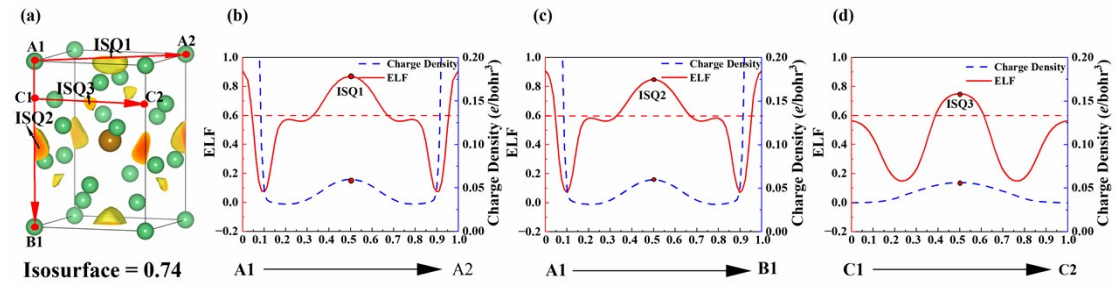


**Fig. S4.** (color online) Variation of the ELF and charge density in  $\text{Be}_{11}\text{Fe}$  along the given paths. The horizontal coordinates in (b), (c) and (d) correspond to the paths from atom A1 to atom A2, from atom A1 to atom B1, and from point C1 to point C2, as shown by the arrows in (a), respectively. The midpoint of these three paths are the location of interstitial charge localization.

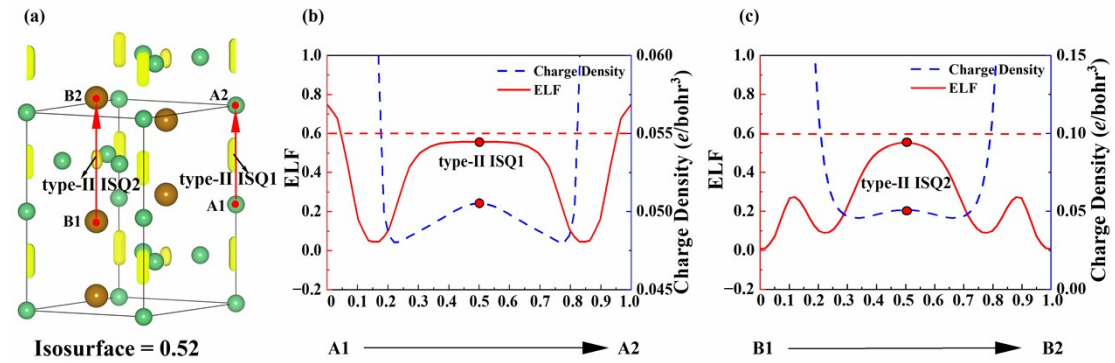


**Fig. S5.** (color online) Variation of the ELF and charge density in  $\text{Be}_2\text{Fe}$  along the given paths. The horizontal coordinates in (b) and (c) correspond to the paths from atom A1 to atom A2 and from atom B1 to atom B2 as depicted by arrows in (a), respectively. The midpoint of both paths are the location of interstitial charge accumulation.

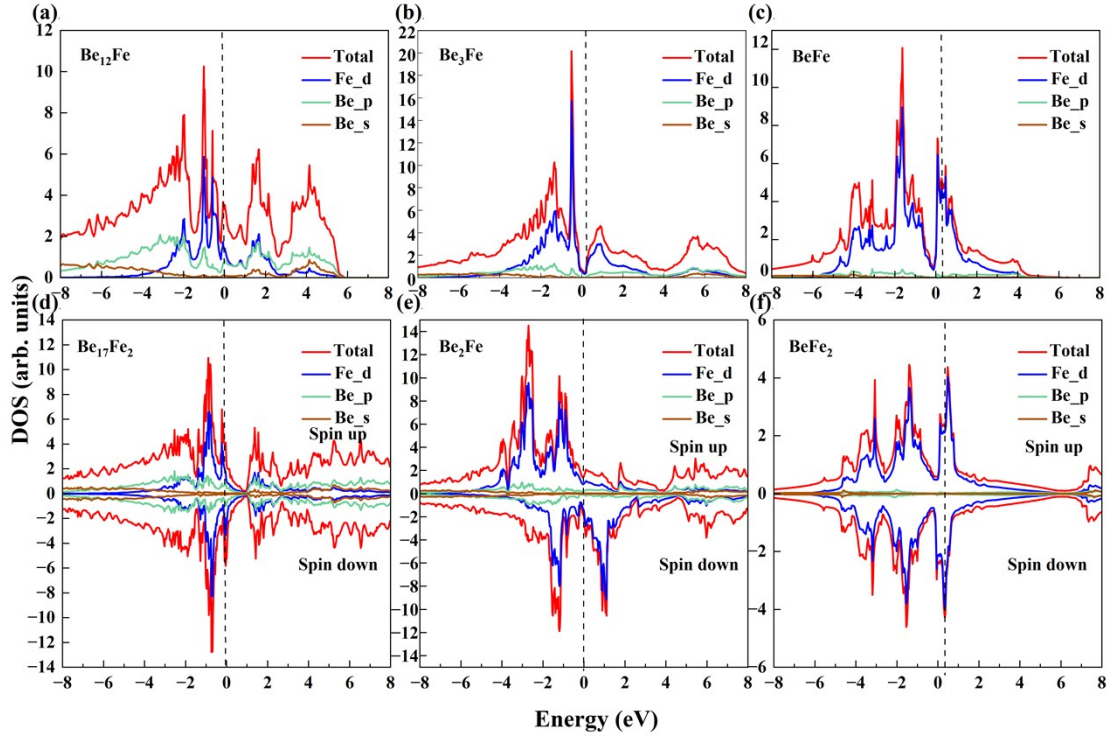


**Fig. S6.** (color online) PDOS of (a)  $\text{Be}_{12}\text{Fe}$ , (b)  $\text{Be}_3\text{Fe}$ , (c)  $\text{BeFe}$ , (d)  $\text{Be}_{17}\text{Fe}_2$  (FM), (e)  $\text{Be}_2\text{Fe}$  (FM), and (f)  $\text{BeFe}_2$  (FM), respectively.

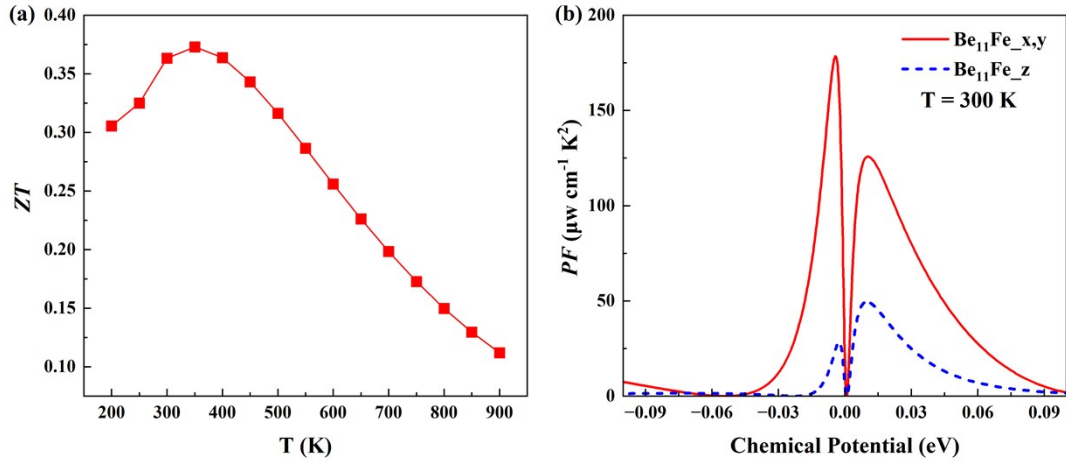


**Fig. S7.** (color online) (a) The optimal value of the figure of merit  $ZT$  obtained by mild hole doping at different temperatures for  $\text{Be}_{11}\text{Fe}$ , (b)  $PF$  of  $\text{Be}_{11}\text{Fe}$  as a function of chemical potential at 300 K.

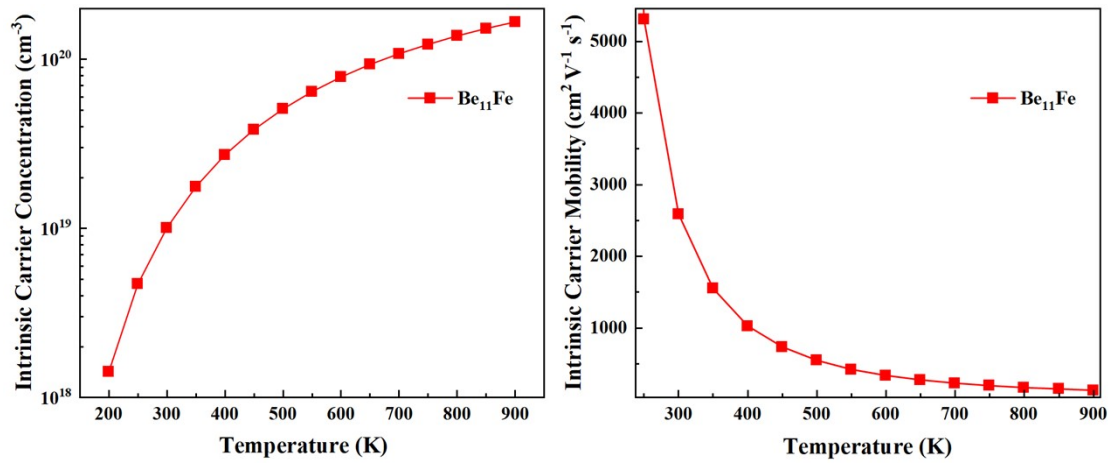


**Fig. S8.** (color online) Intrinsic carrier concentration (left) and intrinsic carrier mobility (right) of Be<sub>11</sub>Fe, respectively.

## Supplementary Tables

**Table S1.** Structural information of the stable and metastable Be-Fe compounds

Phase	Lattice parameters (Å)	Atom	Wyckoff site	Bader charge (e <sup>-</sup> )	Atomic coordinates (fractional)	
<b>Be<sub>12</sub>Fe- I4/mmm</b>	a = b = 7.145 c = 4.083 $\alpha = \beta = \gamma = 90.000$	Be	8f	-0.919	0.250 0.250 0.250	
			8i	-1.025	0.348 0.000 0.000	
			8j	-0.865	0.290 0.500 0.000	
		Fe	2a	0.420	0.000 0.000 0.000	
<b>Be<sub>17</sub>Fe<sub>2</sub>- P6m2</b>	a = b = 4.090 c = 10.628 $\alpha = \beta = 90.000$ $\gamma = 120.000$	Be	2i	-0.960	0.667 0.333 0.100	
			1a	-0.784	1.000 0.000 0.000	
			1c	-0.643	0.333 0.667 0.000	
			2g	-1.182	0.000 1.000 0.370	
			2h	-1.165	0.333 0.667 0.344	
			3k	-1.127	0.990 0.494 0.500	
			6n	-0.982	0.166 0.834 0.185	
		Fe	2i	2.716	0.667 0.333 0.307	
<b>Be<sub>11</sub>Fe- P4m2</b>	a = b = 4.108 c = 5.785 $\alpha = \beta = \gamma = 90.000$	Be	1a	-0.582	0.000 1.000 1.000	
			2g	-1.146	1.000 0.500 0.256	
			4j	-1.138	0.744 0.000 0.382	
			4k	-1.078	0.500 0.255 0.133	
					Fe	1c
<b>Be<sub>5</sub>Fe- F43m</b>	a = b = c = 5.825 $\alpha = \beta = \gamma = 90.000$	Be	4c	-1.107	0.250 0.250 0.250	
			16e	-1.125	0.374 0.126 0.874	
					Fe	4a
<b>Be<sub>4</sub>Fe- C2/c</b>	a = 7.716 b = 4.101 c = 7.690 $\alpha = \gamma = 90.000$ $\beta = 137.384$	Be	8f	-1.188	-0.308 -0.074 0.145	
			8f	-1.231	0.605 0.395 0.953	
					Fe	4e
<b>Be<sub>3</sub>Fe- Pmmn</b>	a = 4.551 b = 3.647 c = 3.777 $\alpha = \beta = \gamma = 90.000$	Be	2b	-1.290	1.000 0.500 0.690	
			4f	-1.199	0.252 0.500 0.163	
			Fe	2a	3.686	0.500 0.500 0.653
<b>Be<sub>2</sub>Fe- P6<sub>3</sub>/mmc</b>	a = b = 4.177 c = 6.692 $\alpha = \beta = 90.000$ $\gamma = 120.000$	Be	2a	-1.004	0.000 0.000 0.000	
			6h	-1.081	0.658 0.829 0.250	
					Fe	4f
<b>BeFe- P4/nmm</b>	a = b = 2.569 c = 5.368 $\alpha = \beta = \gamma = 90.000$	Be	2c	-1.190	-0.000 0.500 0.109	
					Fe	2c
<b>BeFe<sub>2</sub>- I4/mmm</b>	a = b = 2.567 c = 8.407 $\alpha = \beta = \gamma = 90.000$	Be	2a	-1.337	0.000 1.000 1.000	
					Fe	4e



### Supplementary references

- [1] C. W. Glass, A. R. Oganov, N. Hansen, USPEX—evolutionary crystal structure prediction. *Comput. Phys. Commun.* **175**, 713-720 (2006).
- [2] G. Kresse, J. Furthmüller, Efficiency of ab-initio total energy calculations for metals and semiconductors using a plane-wave basis set. *Comput. Mater. Sci.* **6**, 15-50 (1996).
- [3] G. Kresse, J. Furthmüller, Efficient iterative schemes for ab initio total-energy calculations using a plane-wave basis set. *Phys. Rev. B* **54**, 11169-11186 (1996).
- [4] H. J. Monkhorst, J. D. Pack, J. D. Special points for Brillouin-zone integrations. *Phys. Rev. B* **13**, 5188 (1976).
- [5] W. Li, J. Carrete, N. A. Katcho, N. Mingo, ShengBTE: A solver of the Boltzmann transport equation for phonons. *Comput. Phys. Commun.* **185**, 1747-1758 (2014).
- [6] P. Giannozzi, S. Baroni, N. Bonini, M. Calandra, R. Car, C. Cavazzoni, D. Ceresoli, G. L. Chiarotti, M. Cococcioni, I. Dabo, A. Dal Corso, S. de Gironcoli, S. Fabris, G. Fratesi, R. Gebauer, U. Gerstmann, C. Gougoussis, A. Kokalj, M. Lazzeri, L. Martin-Samos, N. Marzari, F. Mauri, R. Mazzarello, S. Paolini, A. Pasquarello, L. Paulatto, C. Sbraccia, S. Scandolo, G. Sclauzero, A. P. Seitsonen, A. Smogunov, P. Umari, R. M. Wentzcovitch, QUANTUM ESPRESSO: a modular and open-source software project for quantum simulations of materials. *J. Phys.: Condens. Matter* **21**, 395502 (2009).
- [7] S. Poncé, E. R. Margine, C. Verdi, F. Giustino, EPW: electron–phonon coupling, transport and superconducting properties using maximally localized Wannier functions. *Comput. Phys. Commun.* **209**, 116-133 (2016).
- [8] G. K. H. Madsen, J. Carrete, M. J. Verstraete, BoltzTraP2, a program for interpolating band structures and calculating semi-classical transport coefficients. *Comput. Phys. Commun.* **231**, 140-145 (2018).